ACS OMEGA

Open Access

This article is licensed under CC-BY-NC-ND 4.0

http://pubs.acs.org/journal/acsodf

Article

Structural Effects of Multivalent Counterions in the Self-Assembly of Polyelectrolyte Copolymers

Liyan Liu,*,§ Fujia Wang,§ Boyi Zhang, Ting Zhang, Ying Wang, and Bing Han

Cite This: *ACS Omega* 2025, 10, 17694−17704

Read Online

ACCESS | Metrics & More | Article Recommendations | Supporting Information

ABSTRACT: In this paper, we investigate the effects of multivalent counterion units and linear counterion chains in the self-assembly of polyelectrolyte (PE) copolymers. Both the valent and structural effects of the counterions are discussed. As the valence of counterion units or the length of counterion chains increases, the electrostatic correlations are significantly strengthened. Compared with multivalent counterion units, the linear structure of counterion chains is primarily manifested in two aspects. First, the electrostatic repulsion among the monovalent ions within the counterion chains diminishes near-neighbor electrostatic correlations, resulting in less compact PE coronas and more stretched PE blocks. Second, the linear arrangement of counterions reinforces the remote spatial electrostatic correlations, prompting the formations of ring-like and semiring-like PE coronas. The charge distribution in the PE coronas closely depends on counterion structures. As the counterion valence or length increases, the enhanced electrostatic effects draw more counterions into the inner regions of the PE coronas. The overcompensation of multivalent counterions within the inner regions of the PE coronas results in local charge inversion. The increased absorption of counterion chains not only raises the positive charge in the inner regions but also extends it to the peripheral regions of the PE coronas, thereby reducing the critical interfacial distance required for the transition in the net charge polarity.

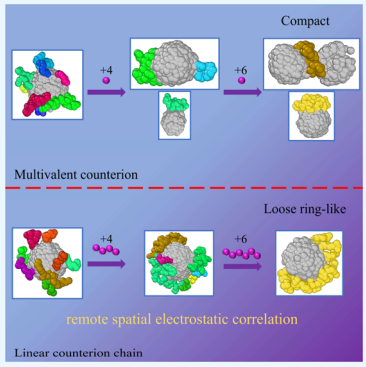

1. INTRODUCTION

The response of block polyelectrolyte (PE) systems to external stimuli such as temperature,[1] electric field,[2,3] salt,[4,5] pH,[6,7] etc. is of great significance in many application areas, including drug delivery,[8−10] nanomaterial fabrication,[11,12] and stabilization of colloidal particles.[13,14] In recent years, the self-assembly of amphiphilic PE copolymers has attracted considerable attentions due to their tunable self-assembled morphologies with practical and potential applications.[15−17] PEs are known to dissociate charged groups in polar solvents like water, resulting in charged polymer chains and the release of counterions into the solution.[18] The assembled morphologies of PE copolymers are more diverse compared to those of their neutral copolymer counterparts. This diversity is mainly due to the presence of long-range electrostatic interactions, which can be regarded as additional means to respond to stimuli.[19−22] As the strength of electrostatic interactions is tuned, phase transitions and structural changes in PE assemblies are observed.[23] With increasing the salt content, re-entrant condensation of the assembled micelles of diblock PEs was observed,[24] and the morphological transition from a micellar network to worm-like aggregates was found for triblock PEs.[25] By adjusting the external electric field, diblock PEs with different block ratios can transform cascade microphase structures, including lamellar, cylindrical, spherical, and disordered phases.[2]

In the self-assembly of PE systems, the property of counterions plays a crucial role.[22,26] The assembled behaviors of block PEs are directly determined by counterion valence. As increasing the counterion valence, the electrostatic repulsions between PE monomers are effectively reduced, and the electrostatic correlations are greatly enhanced, inducing the formations of chain-like and planar-like superstructures, which are not observed in the presence of monovalent counterions.[24] A stable phase of toroidal supramolecular micelle was found in the self-assembly of triblock copolymers, the interaction of negatively charged hydrophilic monomers with divalent organic counterions is the key factor to toroid micelle formation.[27] The effect of trivalent counterions led to the collapse of PE brushes into octopus-like micelles.[28,29] In addition to the valence, the size of the counterion also plays an important role in the assembly of PEs. As the size of the counterion decreased, the counterions were strongly bound to the charged monomers, forming ion pairs and multiplets.[30,31] Much weaker solvation of larger counterions was exhibited in water, which enhances the electrostatic attractions between PE monomers and counterions, and microscopic aggregation of ionic species was found.[30] Both the swelling of PE brushes and

Received: January 1, 2025
Revised: March 29, 2025
Accepted: April 9, 2025
Published: April 27, 2025

ACS Publications

© 2025 The Authors. Published by American Chemical Society

https://doi.org/10.1021/acsomega.5c00002
ACS Omega 2025, 10, 17694−17704

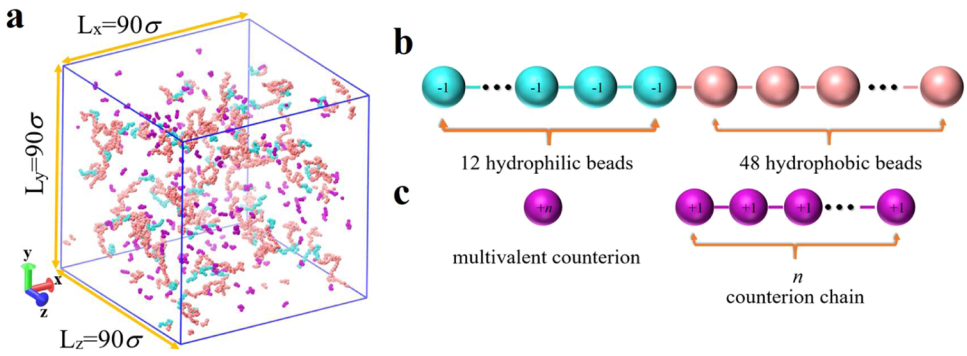

Figure 1. Schematic representation of (a) a simulated cubic box, (b) a PE copolymer, and (c) a multivalent counterion and a linear counterion chain. Black beads represent omitted parts.

the assembled behaviors of block PEs showed large dependences on the type and size of counterions.[32−35]

The length of the counterions also plays an important role in determining the electrostatic interactions. The assembled structures of triblock PE copolymers were tuned by the length of organic counterionic diamine hydrophilic spacer, flat disk micelles were produced with shorter linkers, and cylinders and spheres were obtained with longer counterions.[36] The volume of micellization of homologous surfactants, *n*-alkylammonium decanesulfonates, and *α*, *ω*-alkanediammonium nonanesulfonates was closely dependent on the length of counterions.[37] The large positive increase in the volume was found with the increase in the counterion chain length.[37] In solution, diamines form divalent cations with a length that can be systematically varied.[38] It was found that shorter diamines can induce the formation of bundles, and longer diamines tend to enhance short-range repulsion and decrease the stability of bundles.[38]

Although the effects of valence, size, and length of counterions have been extensively investigated, the role of the structure of the counterion is not yet clear. Herein, we investigate the influences of the counterion structure on the assembled behaviors of block PEs. Two types of counterions are considered: single multivalent counterion units and linear counterion chains composed of monovalent ions. The valent effects are discussed by increasing the valence or the chain length of counterions, and the effects of the counterion structure on the properties of the self-assemblies are discussed in comparisons. In experiments, multivalent counterions and counterion chains cannot be directly released during the ionization process; they should be introduced as components of salt solutions. However, when the content of multivalent counterions in the salt solution can exactly neutralize the PE system, due to stronger electrostatic correlations induced by multivalent ions and counterion chains, they act as the primary counterions interacting with the PE system, and the assemblies closely resemble those formed when multivalent ions are utilized as direct counterions.[24] Therefore, the effects of multivalent ions and ion chains can be qualitatively investigated as counterions without salt.

The organization of the paper is as follows. The model, methods, and simulation details are introduced in Section 2. In Section 3, the self-assembly behaviors of PE diblock copolymers in the presence of multivalent counterions and counterion chains are systematically studied, and both the valent and the structural effects are discussed. Finally, the conclusions are presented in Section 4.

2. SIMULATION MODEL AND DETAILS

2.1. Simulation Model. The self-assembly behaviors of two-block PEs in the presence of multivalent counterion units and counterion chains are discussed, respectively. The block PE polymers are represented by a coarse-grained model of flexible chains denoted as $A_{12}B_{48}$, as shown in Figure 1b, where A represents the hydrophilic PE block with each monomer carrying a negative unit charge, and B represents the neutral hydrophobic block. The polymerization of PE block is 12 and of the hydrophobic block is 48. In order to maintain electrical neutrality within the PE system, multivalent cations or linear polycation chains, where each monomeric unit bears a positive charge, are employed as counterions, as shown in Figure 1c. The valence of a single multivalent unit is denoted as Z_C, and the number of monovalent ions in a counterion chain is marked as N_C. Divalent to hexavalent counterions are considered in these two cases. The simulation was carried out in a cubic box with side lengths $Lx = Ly = Lz = 90\sigma$, with periodic boundary conditions in all directions, as shown in Figure 1a. The monomer density ρ of copolymer monomers is fixed at $0.005/\sigma^3$.

2.2. Parameterization of Interparticle Interactions. The neighboring beads on the same chains are connected by the finite extensible nonlinear elastic (FENE) potential,[39] modeling the bonding interactions both in polymer chains and counterion chains

$$U_{\mathrm{FENE}} = -\frac{1}{2}kR_0^2\ln\left[1 - \left(\frac{r}{R_0}\right)^2\right] \quad (1)$$

with a spring constant $k = 30k_BT/\sigma^2$ and a maximum extensible bond length $R_0 = 1.5\sigma$,[40] where σ is the diameter of the particles, assumed to be the same irrespective of particle type as a simplification.

The angle bending potential for the rigid chains can be described by a cosine/delta function,

$$U_\theta = k_\theta[1 - \cos(\theta - \theta_0)] \quad (2)$$

where k_θ is the angle spring constant, θ is the angle between every two consecutive bonds, and θ_0 is the chain equilibrium angle. The larger the k_θ value, the more rigid the molecule chain. The magnitude of the constant k_θ is set to 0 for flexible chains, and the equilibrium angle is set to 180°.

van der Waals interactions between particles are represented by shifted and truncated Lennard-Jones (LJ) potentials[41]

https://doi.org/10.1021/acsomega.5c00002
ACS Omega 2025, 10, 17694−17704

$$U_{LJ} = \begin{cases} 4\varepsilon_{LJ}\left[\left(\frac{\sigma}{r_{ij}}\right)^{12} - \left(\frac{\sigma}{r_{ij}}\right)^{6} - \left(\frac{\sigma}{r_c}\right)^{12} + \left(\frac{\sigma}{r_c}\right)^{6}\right] & r_{ij} < r_c \\ 0 & r_{ij} > r_c \end{cases} \quad (3)$$

where r_{ij} is the distance between the i-th particle and the j-th particle, ε_{LJ} is the depth of the LJ potential, and r_c denotes the cutoff radius. For A-A and B-B polymer monomers, the cutoff distance is set as $r_c = 2^{1/6}\sigma$ and $r_c = 2.5\sigma$, which corresponds to a good and bad implicit solvent condition for A and B block, respectively, and energy parameters are selected as $\varepsilon_{LJ} = 0.5\ k_BT$ and $\varepsilon_{LJ} = 2.0\ k_BT$. For all other pairs of beads, the parameters r_c and ε_{LJ} are set as $r_c = 2^{1/6}\sigma$ and $\varepsilon_{LJ} = 1.0\ k_BT$ to represent full repulsion interactions (Table 1). The combination of the LJ and the FENE has potential to prevent chain crossings.[42]

Table 1. Selection of Parameters for LJ Interactions among Particles

particle	ε_{LJ}	σ	r_c
A-A	0.5 k_BT	1.0σ	$2^{1/6}\sigma$
B-B	2.0 k_BT	1.0σ	2.0σ
other	1.0 k_BT	1.0σ	$2^{1/6}\sigma$

The electrostatic interaction between any two charged particles q_i and q_j is described by the Coulomb potential energy

$$U_{Coul}(r_{ij}) = k_BT\frac{\lambda_B q_i q_j}{r_{ij}} \quad (4)$$

where k_B is the Boltzmann constant, T is the absolute temperature, $\lambda_B = e^2/4\pi\varepsilon_0\varepsilon_r k_BT$ is the Bjerrum length, e is the elementary charge, ε_0 is the vacuum permittivity, and ε_r is the relative dielectric constant of the solvent. In water and at room temperature, the Bjerrum length is $\lambda_B = 7.1$Å; in our simulation, we set $\lambda_B = 3\sigma$, therefore $\sigma = 2.4$Å, and the number density of polymer monomers is 3.6×10^{-4}/Å^3. Coulomb long-range interactions are calculated by using the particle−particle/particle−mesh (PPPM) algorithm with an estimated accuracy of 10^{-3}.[43]

2.3. Simulation Details. The Open-Source software LAMMPS[44] is used to perform the simulations under the canonical (NVT) ensemble. The system is coupled to a Langevin thermostat to maintain a constant temperature[45] $T = 1.0\ \varepsilon_{LJ}/k_B$ (corresponds to room temperature 298 K). The motion of a particle is described by the Langevin equation

$$m\frac{d^2\vec{r_i}(t)}{dt^2} = -\nabla U_i - \xi\frac{d\vec{r_i}(t)}{dt} + \vec{F}_i^R(t) \quad (5)$$

where m and U_i are the mass of the particle and the total potential energy of the system, respectively. $\xi = 1.0\ m\tau^{-1}$ is the friction coefficient, where τ is the standard LJ time $\tau = \sigma(m/\varepsilon_{LJ})^{1/2}$. The random force $F_i^R(t)$ satisfies the fluctuation−dissipation theorem and has a zero average value. For simplicity, we assume that all particles have the same mass, $m = m_0$. The standard LJ units are used to represent all physical quantities, which means that all quantities are based on fundamental quantities: mass (m), distance (σ), and energy (ε_{LJ}). The motion of beads is solved by the Velocity-Verlet algorithm,[46] and the value of the integration time step is set as $\Delta t = 0.005\tau$. Initially, a softening potential function in the form of cosine is applied to all the particles to separate the overlapping particles and produce a random distribution of polymer chains and counterions.[47]

The system is equilibrated 2.0×10^7 steps until the time evolution of thermodynamic quantities reaches a stable state regime, and little fluctuation is observed in the total energy of the system, as shown in Figure 2. Thus, one may believe the system has reached a steady state. After the equilibrium run, another 4×10^6 steps are performed for production samples, and 1001 configurations are saved for further analysis. Each set of experiments is repeated three times, and data are shown as the mean ± SD (standard deviation). Since similar results are obtained in the three replicas, we show only the structures in one replica.

3. RESULTS AND DISCUSSION

In the presence of monovalent counterions, the electrostatic attraction between PE monomers and monovalent counterions is relatively weak. Consequently, not all of the counterions are bound by the PE chains, giving rise to the formation of micellar aggregates characterized by a dilute and expansive corona, as illustrated in Figure S1. An increase in Z_C (or N_C) intensifies the electrostatic attractions of counterions; more PE monomers are derived together by a single counterion (or a counterion chain). The enhancement in electrostatic interactions boosts the correlation among PE monomers, thereby causing the PE coronas to become more condensed,

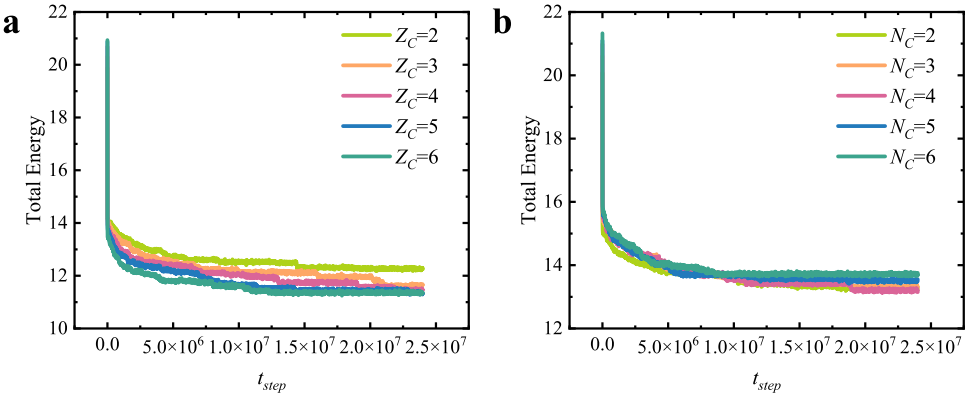

Figure 2. Energies of the total system in the presence of different types of counterions, (a) multivalent counterions, and (b) counterion chains.

https://doi.org/10.1021/acsomega.5c00002
ACS Omega 2025, 10, 17694−17704

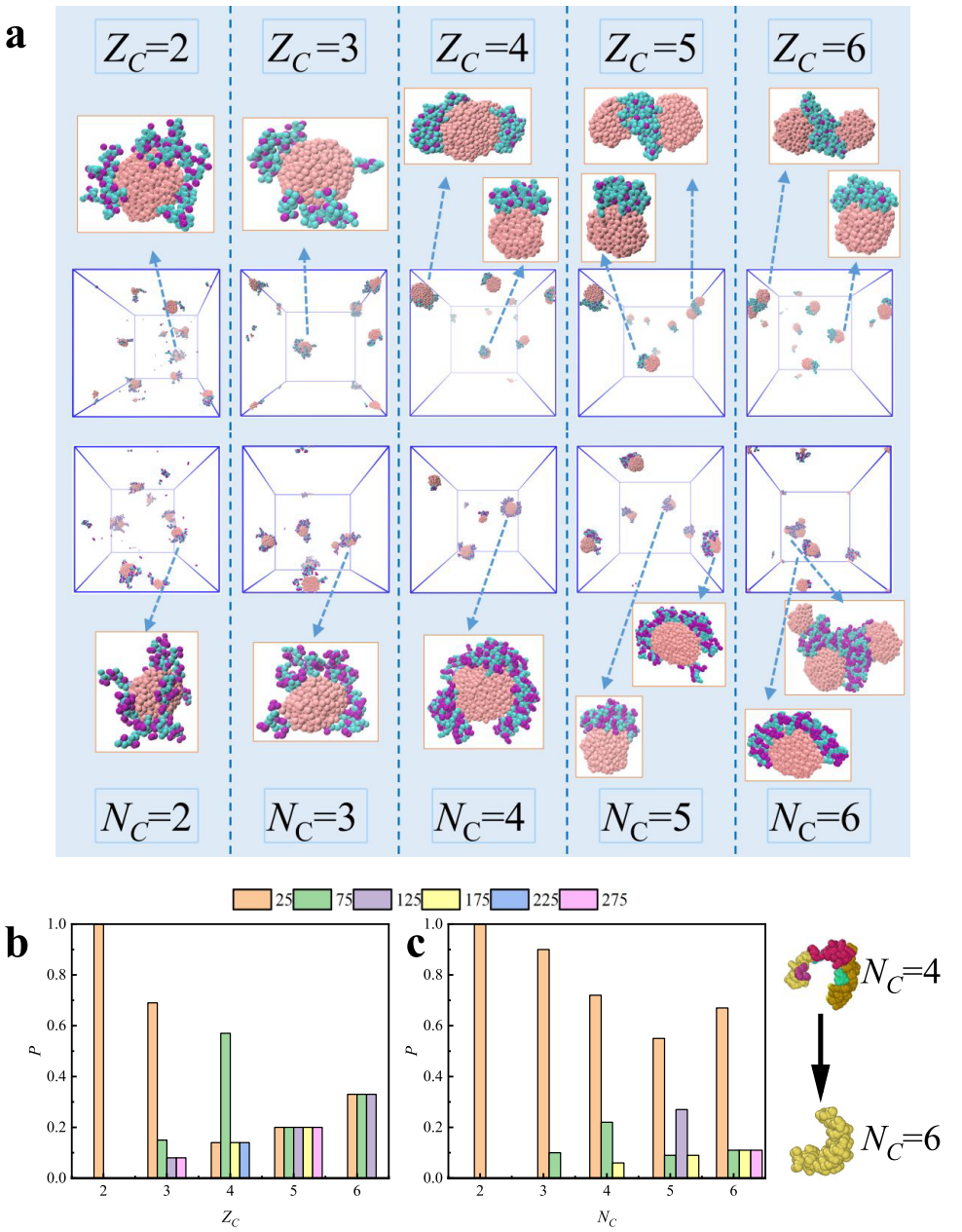

Figure 3. Snapshots of the self-assemblies of PE copolymers in the presence of multivalent units and counterion chains are shown in the upper and lower parts of panel (a), respectively. The PE monomers, hydrophobic beads, and counterions are shown in cyan, pink, and purple colors, respectively. The size probability distributions of assembled PE clusters in the presence of multivalent counterion units and counterion chains are shown in panels (b) and (c), respectively. The different colors represent the different sizes.

particularly in the presence of multivalent counterions, as shown by the snapshots of the assembled structures in Figure 3a. At low valences, Z_C (or N_C) = 2 and 3, similar assembled structures are observed in the presence of these two types of counterions. However, as the valence increases, the impact of the counterion structure becomes more pronounced. Compared with multivalent counterion units, the electrostatic repulsion between ions along the counterion chains diminishes the effect of neighboring electrostatic correlations, and the PE coronas assembled in the presence of counterion chains are less compact than those formed with multivalent units, evidenced by the rightward shift and the broadening of the main peak in radial distribution function (RDF) between hydrophobic and PE monomers (as shown in Figure S2a,b). Strong electrostatic correlation mediated by quadrivalent counterion units triggers the cross-linking of PE blocks, giving rise to the formation of patch-like coronas. Consequently, spherical micelles with one or two compact PE patches are formed. At N_C = 4, the enhanced electrostatic effect also facilitates the adsorption of PE blocks together; meanwhile, the weaker near-neighbor electrostatic correlations prevent the excessive aggregation of PE chains. Moreover, the strengthened remote spatial electrostatic correlations enable the PE chains to behave like ropes, binding more PE chains together. These combined effects contribute to the formation of PE clusters encircling the hydrophobic core. As a result, micelles with ring-like PE coronas are presented, as demonstrated in the snapshot. In the presence of higher valent counterions or

https://doi.org/10.1021/acsomega.5c00002
ACS Omega 2025, 10, 17694−17704

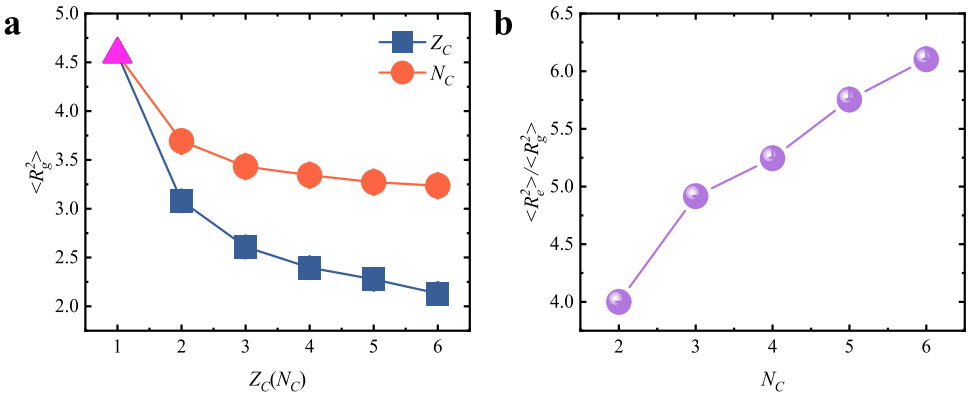

Figure 4. (a) Radii of gyration of PE block with counterions, (b) $\langle R_e^2 \rangle \langle R_g^2 \rangle$ of counterion chains.

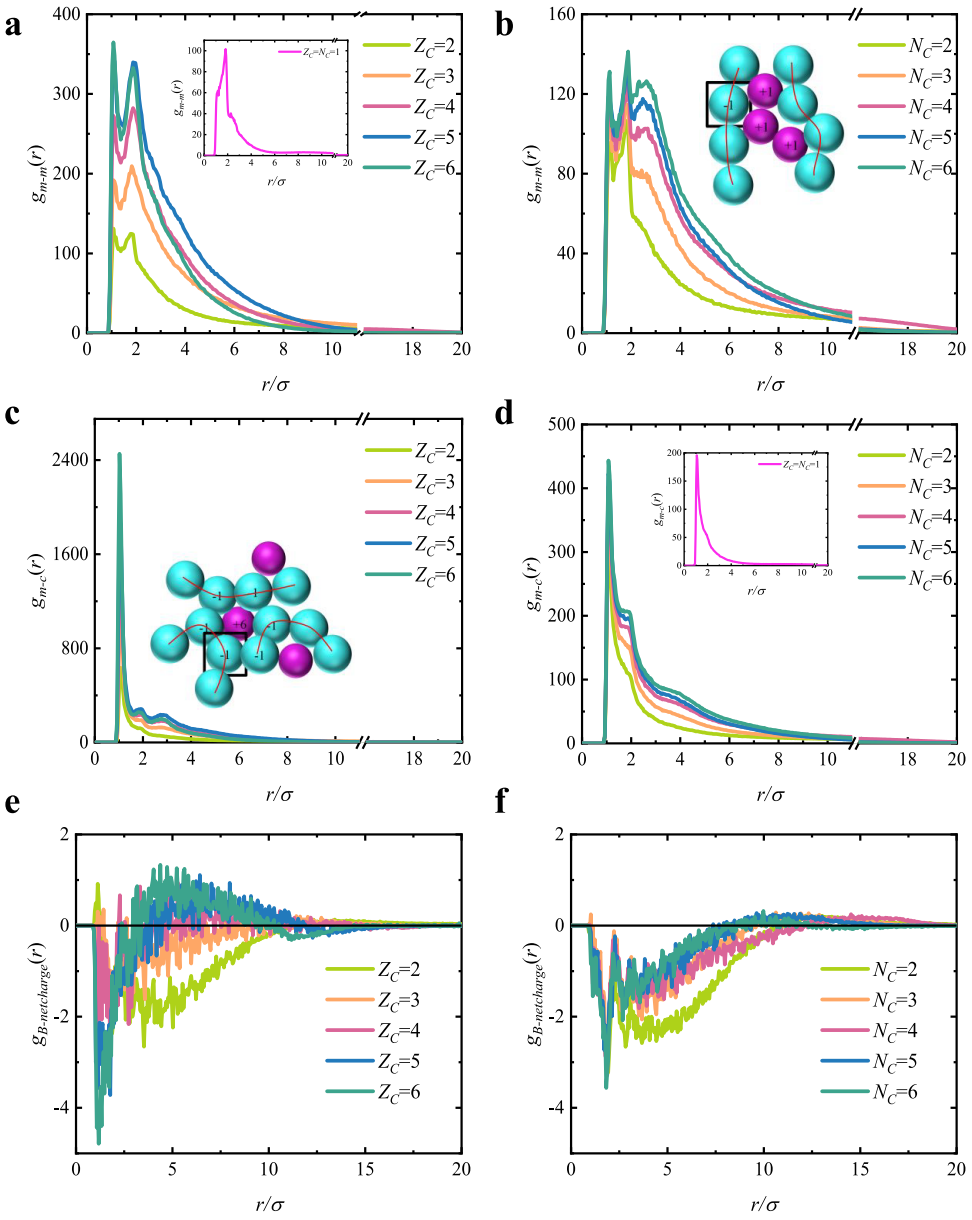

Figure 5. RDFs between PE monomers−monomers at (a) multivalent counterions and (b) counterion chains and between PE monomers−counterions at (c) multivalent counterions and (d) counterion chains. Net charge distributions at (e) multivalent counterions and (f) counterion chains. Cartoon plots in panels (c) and (b) illustrate the way of condensation of multivalent counterions and counterion chains, respectively. The RDFs between PE monomer−monomer and PE monomer−counterion in the presence of monovalent counterions are shown in the subplots of panels (a) and (d), respectively.

https://doi.org/10.1021/acsomega.5c00002
ACS Omega 2025, 10, 17694−17704

longer counterion chains, the stronger electrostatic interactions render more compact PE patch coronas, and the correlation between micelles is aroused. Once the distance between micelles is close enough, the bridging effect of the externally dispersed counterions is activated, triggering intermicellar cross-linking. Subsequently, the micelles reorganize their PE corona structures and cross-link together, inducing the formation of micelle dimers and even multimers. The processes of the cross-linking of micelles are shown in Figure S3. Micelle dimers are identified at pentavalent and hexavalent counterion units, and the micelle trimer is observed with counterion chains at $N_C = 6$. An increase in the length of the counterion chains enhances their capacity to adsorb a greater number of PE monomers, which leads to a transformation of the ring-shaped PE coronas observed at $N_C = 4$ into semicircular configurations at $N_C = 5$ and 6.

A cluster is defined as a set of connected particles, each of which is within the reach of the other particles in the same cluster.[48] The stronger electrostatic correlation induced by multivalent counterions, as compared with counterion chains, is further demonstrated by the assembled PE clusters (Figures 3b,c and S4), and more big-sized PE clusters are found in the presence of multivalent counterion units. The enhanced remote spatial correlation of counterion chains is also illustrated by the fusion of PE clusters with increasing chain length, as shown in Figure 3c.

The radii of gyration of PE blocks are discussed to further study the effects of the counterions (Figure 4a). The electrostatic repulsions among the PE monomers within the polymer chains are insufficiently mitigated in the presence of monovalent counterions, thereby giving rise to an elongated conformation of the PE chains. As the valence of the counterion, Z_C, increases, a single multivalent counterion unit is capable of adsorbing a larger number of PE monomers collectively, which pronouncedly enhances the scale of electrostatic shielding, leading to deep collapses of PE chains, and thus, the radius of gyration of PE chains in the presence of multivalent counterion units shows a significant decrease. In the presence of counterion chains, the electrostatic repulsion between the ions along the counterion chains elongates the conformation of the counterion chains, as shown in Figure 4b. As the counterion chain length, N_C, increases, although more PE monomers are attracted by a counterion chain, the imposed structural constraints of bonded counterions hinder the compact accumulation of PE monomers, and a relatively slight decrease in the radius of gyration of PE chains is presented.

To better explore the effects of multivalent counterions on the self-assemblies of PE copolymers, we comparatively discuss the RDFs for PE monomers around each PE monomer $g_{m-m}(r)$ in the presence of multivalent counterion units and counterion chains, as shown in Figure 5a,b, respectively. An increase in counterion valence directly enhances the electrostatic adsorption of PE monomers, leading to the accumulation of PE monomers; consequently, the correlation between PE monomers mediated by multivalent counterion units is greatly intensified, as demonstrated by the increased peak values and steepened tails in Figure 5a. The peaks located at $r = 1.0\sigma$ and $r = 2.0\sigma$ in $g_{m-m}(r)$ mainly originate from the PE monomers that are directly connected through covalent bonds and the bridged monomers mediated by counterions, respectively.[28] The notable increment of these two peak values implies a substantial near-neighbor accumulation of PE monomers around a PE monomer, which elucidates the clustering effect of PE monomers. In the context of counterion chains, the structural constraints imposed on the bonded counterions play an important role in shaping the spatial electrostatic correlations. In addition to the two prominent peaks, a third notable peak located at $r = 3.0\sigma$ is observed in $g_{m-m}(r)$ at $N_C > 3$. The adsorption of PE monomers by those bonded counterions gives rise to the emergence of a third peak in $g_{m-m}(r)$, as illustrated by the inset cartoon plot in Figure 5b. The effect of the chain structure of counterions can be manifested through near- and remote spatial electrostatic correlations. The slight increase in the near-neighbor correlation, as indicated by the first two peaks, suggests that the attractions induced by counterion chains are not strong enough to convene the PE monomers in an extremely compact manner. In other words, these attractions do not significantly enhance the aggregation of polymer monomers in their immediate vicinity. On the other hand, a marked improvement in the distant correlation, as portrayed by the increased third peak values, indicates that the chain length augments the spatial correlation over a larger distance.

The RDFs for counterions around each PE monomer $g_{m-c}(r)$ in the presence of multivalent counterion units and counterion chains are shown in Figure 5c and d, respectively. An increase in counterion valence directly strengthens the aggregation of PE monomers, and the strong electrostatic correlation between PE monomers is induced, as demonstrated by the appearance of the third peak in $g_{m-c}(r)$ (Figure 5c). In the presence of counterion chains, the second main peak in $g_{m-c}(r)$ becomes significantly prominent compared with its counterpart with multivalent counterions. The imposed structural effect of counterion chains is depicted; when the PE monomers are adsorbed by counterion ions, the monomer ions bonded to the adsorbed ones in counterion chains contribute to the pronounced second peak in $g_{m-c}(r)$, as demonstrated by the inset cartoon plot in Figure 5b.

The RDF between the hydrophobic monomers and the PE monomers elucidates the distribution of negative charges surrounding the hydrophobic particles. In a parallel manner, the RDF between the hydrophobic monomers and counterions reveals the spatial arrangement of positive charges. The discrepancy between these two functions can delineate the net charge distribution around the hydrophobic particles,[49] denoted as

$$g_{\text{B-netcharge}}(r) = \begin{cases} \dfrac{n_C}{n_A} \times Z_C \times g_{\text{B-C}}(r) & \text{for multivalent counterions} \\ \quad - g_{\text{B-A}}(r) & \\ g_{\text{B-C}}(r) - g_{\text{B-A}}(r) & \text{for counterions chains} \end{cases} \tag{6}$$

where n_C and n_A are the number densities of multivalent counterions and PE monomers, respectively. The net charge distribution around the hydrophobic particles in the presence of counterion chains and multivalent counterions is shown in Figure 5e and f, respectively. Due to the repulsive interactions between particles, counterions are unable to be adsorbed in very close proximity to the PE monomers, within the range of $r < 1.0\sigma$ around the hydrophobic beads; the net charge is always negative. When Z_C or N_C is less than four, the electrostatic interaction is insufficient to attract an adequate number of

https://doi.org/10.1021/acsomega.5c00002
ACS Omega 2025, 10, 17694−17704

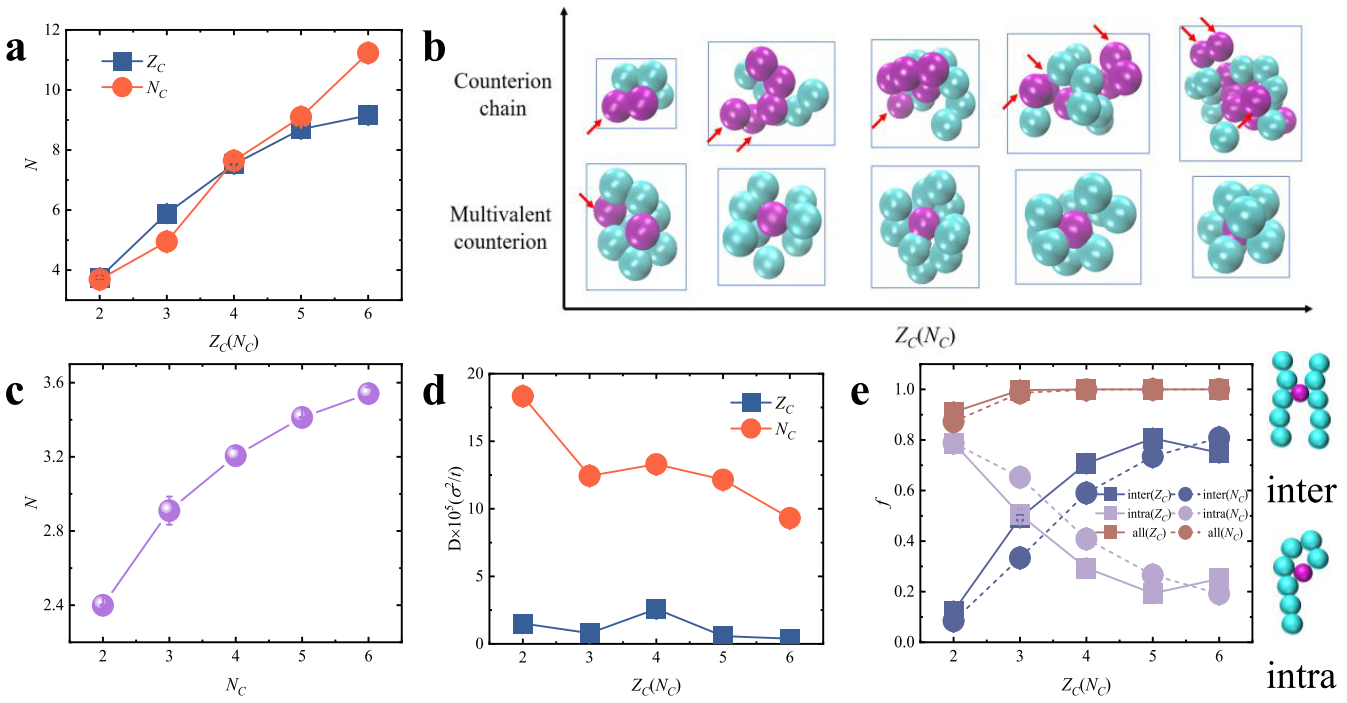

Figure 6. (a) Average coordination number of PE monomers around a counterion unit and a counterion chain. (b) Snapshots of PE monomers residing in the first shell around the central counterions. The counterions highlighted by the red arrow represent additional counterions that are not taken into account in the first shell of the central beads. (c) Average coordination number of PE monomers around a monovalent ion in the counterion chains. (d) Diffusion coefficients of counterions. (e) Condensation ratios of multivalent counterions and counterion chains. The cartoon illustrates the two states of interchain and intrachain bridging of counterions.

counterions into the inner region of the PE coronas; consequently, the inner region assumes a negative charge, while the outer peripheries remain positive. As Z_C or N_C increases, the electrostatic attraction between PE monomers and counterions is intensified, and more counterions are attracted into the inner regions of PE coronas near the hydrophobic core; thus, the negative charge within the inner region of PE coronas near the hydrophobic core is gradually decreased, and the positive charge within the outer propensity is also reduced. At $Z_C = 4$, the electrostatic neutrality is nearly achieved in the inner region of PE coronas, and as $Z_C > 4$, the local charge inversion appears, the charge in the inner regions of PE coronas is over compensated and turns positive. For high-valent counterion units, the electrostatic screening scale is enlarged, and a large amount of PE monomers needs to be adsorbed to reduce the electrostatic energy. Given that the density of PE monomers near the hydrophobic core is higher than the density in the outer region, multivalent counterions are inclined to reside within the inner region of the corona. Consequently, regional disparities in charge compensation are aroused. The more densely populated counterions in the inner sectors of PE coronas lead to excessive charge neutralization, and the inadequate neutralization in the outer regions results in overall negative charge. With regard to counterion chains, the imposed structural effect influences the charge distribution. As the counterion chain length increases, the space they occupy becomes larger; the increased absorption of counterion chains not only raises the positive charge in the inner regions but also extends it to the outer regions of the PE coronas, thereby diminishing the critical distance required for the transition in net charge polarity. As compared with multivalent counterion units, the imposed linear structure of counterions weakens the electrostatic correlation and reduces the screening scale, significant local charge reversion is not observed in the presence of counterion chains, and the net charge in the outer peripheries of the PE coronas always keeps positive.

The coordination number is used to describe the average number of atoms within the first shell around the central atom, depicting the closeness of the particle arrangement in the system. The coordination number can be obtained by integrating the first peak of the radial distribution function,[50,51] which is defined as

$$N = \int_0^{r_{min}} g(r) 4\pi\rho r^2 \mathrm{d}r \tag{7}$$

The average coordination number of PE monomers around a multivalent counterion unit initially shows a rapid growth with Z_C, and subsequently, a more gradual rise is witnessed, as shown in Figure 6a. As Z_C increases, more PE monomers are collectively adsorbed by a multivalent counterion unit, and the PE monomers tightly wrap around the counterions, as depicted in Figure 6b. Consequently, the correlation between counterion units and PE monomers is greatly enhanced, leading to a substantial initial increase in the coordination number of PE monomers. Once the number of PE monomers in the first shell around the counterion units reaches a sufficiently high level, the excluded volume effect and the electrostatic repulsions among the PE monomers come into play. These factors restrict the further accumulation of PE monomers, resulting in a slower increase in the coordination number. For the counterion chains, as N_C increases, the strengthened electrostatic correlation enables them to attract more PE monomers. Additionally, their stretched configuration enables them to accommodate a larger number of PE monomers, as shown in Figure 6b. Therefore, the coordination number of PE monomers for a counterion chain shows a progressive

https://doi.org/10.1021/acsomega.5c00002
ACS Omega 2025, 10, 17694−17704

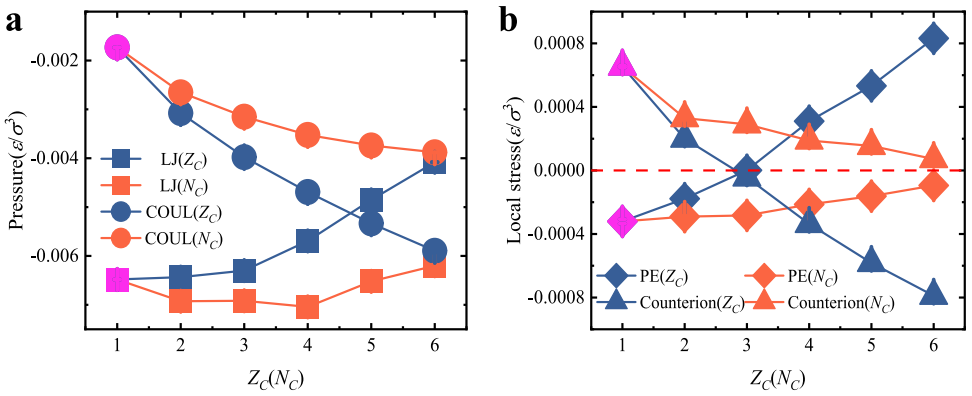

Figure 7. (a) Total pressures of all atoms contributed from LJ and Coulomb interactions. (b) Local stresses of each counterion and PE monomer.

ascension, and it is even greater than that for a multivalent counterion unit as $N_C > 4$. Moreover, the average coordination number for a monovalent ion in the counterion chains also increases with the chain length, as shown in Figure 6c.

To characterize the effects of counterions on the microscopic dynamical properties of the self-assemblies, we calculate the mean-square displacements (MSD) of the counterions in Figure S5 and further obtain the diffusion coefficients of counterions through the slope fitting[52] of $D = \lim_{t\to\infty} \frac{dMSD(t)}{6dt}$ in Figure 6d. As the length of the counterion chains increases, the electrostatic attraction between PE monomers and counterion chains is greatly enhanced. The strengthened adsorption by the PE blocks, coupled with the increased chain length, constrains the mobility of the counterion chains. Consequently, the diffusion coefficient of counterion chains exhibits a great decrease with increasing N_C. For multivalent counterion units, even at low valences, most of them are strongly bound to PE monomers, greatly restricting their mobility; therefore, a slight decrease in the diffusion coefficient is demonstrated with increasing Z_C. Due to the association between PE monomers and counterion chains being based on monovalent interactions, which are relatively weak, the diffusivity of counterion chains is stronger than that of multivalent units, even at long chain lengths. Strong diffusion of particles implies great displacement from their original locations. Due to the strong diffusivity of the counterion chains, the ring-like configurations of PE coronas mediated by counterion chains are not robustly stable. Instead, a dynamic interconversion between ring-shaped coronas and broken annular patch coronas is observed, as shown in Figure S6. In the presence of multivalent counterion units, the strong attraction by PE blocks greatly constrains the motility of multivalent counterions, ensuring the stability of the assembled patchy coronas mediated by multivalent units.

The condensations of counterions as a function of valence or ion number are studied in Figure 6e. Due to the absence of a distinct boundary between the condensation region and the noncondensation area, the condensation region can only be qualitatively described. We believe a counterion is condensed by the PE chains if the distance between it and any charged PE monomers is less than $\sqrt{2}\sigma$.[53] The condensed counterions can be classified into two states: interchain correlation and intrachain condensation.[43] If a counterion monomer is simultaneously absorbed by multiple PE chains, interchain correlation is believed to be observed. In contrast, if a counterion monomer is exclusively condensed by a single PE chain, it is referred to as intrachain condensation. The cartoon plot of the state of counterions monomers is shown in Figure 6e.

The condensation ratio, denoted as f, is defined as the proportion of condensed ions relative to the total number of ions of the same type present. In terms of condensation ratios, similar effects are exhibited by multivalent counterions and counterion chains. At $Zc = 2$ (or $N_C = 2$), most of the counterions are adsorbed by PE monomers, effectively reducing the electrostatic repulsions. Thereafter, nearly all of the counterions are adsorbed under enhanced electrostatic interactions. Intrachain condensation plays the main role as $Z_C < 4$ (or $N_C < 4$) to reduce the electrostatic repulsions along the PE chains; as $Z_C > 4$ (or $N_C > 4$), the interchain correlation becomes dominant. As the simulation progresses and the system evolves toward stability, there is a shift from intrachain to interchain condensation of counterions, as shown in Figure S8, the intrachain condensation ratio decreases, and interchain correlation increases. This shift is indicative of a more energetically favorable configuration, as evidenced by a decrease in the total energy of the system and the energy interactions between the PE monomers and counterions. Therefore, the transition toward interchain condensation is favorable in the system's progression toward a stable state.[54] The strong interchain correlation induces the cross-linking of PE chains, leading to the formation of patchy or ring-like PE coronas. Attributed to the stronger electrostatic effects induced by multivalent counterion units, the interchain correlation ratio of multivalent counterion units is higher than that of counterion chains.

The significance of multivalent counterion units and counterion chains are further discussed through the analysis of pressure.[55,56] The total pressures of all atoms contributed from LJ, Coulomb interactions, bond, and kinetic energies are discussed, respectively (Figures 7a and S7). Increasing counterion valence Z_C or chain length N_C strengthens the electrostatic attraction between PE monomers and counterions, which leads to an increase in the negative contribution to pressure. The impact of Coulomb interactions on the pressure increases significantly with increasing Z_C, in contrast, the increment is relatively modest with increasing N_C. The linear arrangement of monovalent counterions induces electrostatic repulsion, which partially reduces the overall electrostatic effects. Negative short-range LJ contribution to pressure confirms the aggregation of hydrophobic blocks. As Z_C and N_C increase, the strengthened electrostatic correlations facilitate more densely packed configurations of PE monomers, particularly in the presence of multivalent counterion units.

https://doi.org/10.1021/acsomega.5c00002
ACS Omega 2025, 10, 17694−17704

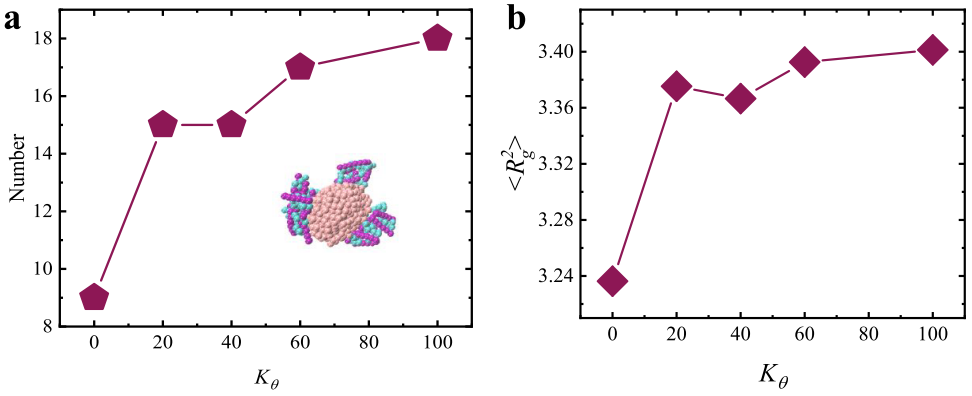

Figure 8. (a) The number of PE clusters and (b) the radius of gyration of PE blocks are plotted as functions of the rigidity of the counterion chain backbone.

This intensified packing leads to stronger short-range LJ repulsions between charged particles, thereby causing the short-range repulsive contribution to show an upward trend with increasing Z_C or N_C. The positive contribution from the bond energy implies the atoms are in a local state of tension, primarily due to the electrostatic repulsions among the bonded PE monomers. Taking into account all the contributions to the overall pressure, it is noted that the system's total pressure nearly approaches zero, suggesting a propensity for local stability.

The local stresses of each counterion and each PE monomer are also discussed in Figure 7b. It clearly shows that as Z_C or N_C increases, the local stress of each PE monomer exhibits an opposite trend to that of the counterions, with the two tendencies nearly compensating for each other. This compensation implies the local stability of the complexation between PE monomers and counterions. In the case of divalent counterion units and chains, the electrostatic binding of counterions is relatively weak; the dispersion of counterions may lead to the presence of positive stresses. As the counterion valence or chain length increases, the electrostatic binding of counterions to PE monomers is significantly enhanced, constraining the movement of counterions; particularly, for multivalent counterion units, the stresses of counterions are effectively reduced. The strong electrostatic correlation mediated by counterions renders the aggregation of PE monomers. This aggregation, in turn, intensifies the repulsions between the PE monomers, leading to an increase in the stress experienced by the PE monomers.

The rigidity of PE chain backbone plays an important role in the self-assembly of PE copolymers.[57] The effect of the rigidity of the counterion chain backbone is further discussed with a fixed chain length N_C = 6. In contrast to their flexible counterparts, rigid counterion chains are less prone to bending, and it is more difficult for them to form complex folded structures, the conformational entropy is reduced, and single conformations of counterion chains are induced, which lead to the presentations of more dispersed PE clusters, as shown in Figure 8a. The ring-like coronas in the presence of flexible counterion chains are absent; instead, patchy-like PE clusters are identified, as illustrated by the inset snapshots in Figures 8a and S9. As the rigidity of counterion backbone intensifies, the energy required for chain bending increases, prompting the chains to adopt a linear configuration. To facilitate the adsorption of these linear counterion chains, the PE chains have to extend to increase the contact area with the rigid counterion chains, consequently expanding the radius of the PE chains, as depicted in Figure 8b. The rigidity of the counterion chains does not inherently affect the condensation ratios; the condensation ratios remain largely stable, as shown in Figure S10.

4. CONCLUSIONS

In this paper, the effects of valence and structure of multivalent counterions on the self-assembly of PE copolymers is studied. Two types of counterions are considered: multivalent counterion units and linear counterion chains composed of monovalent ions.

As compared to multivalent counterion units, the linear arrangement of monovalent ions induces a weaker near-neighbor electrostatic correlation but a stronger remote spatial correlation. Consequently, the PE coronas assembled in the presence of counterion chains are less dense than those formed by multivalent units, and ring-like or semiring-like PE coronas are observed with counterion chains, which are not observed with individual units. The configuration stability of PE coronas depends on the counterions structure. Ion chains, bound by relatively weaker monovalent electrostatic interactions, exhibit greater diffusion and lead to less stable PE corona structures. In contrast, the strong attraction between multivalent counterions and PE monomers restricts unit mobility, yielding stable, compact PE patchy coronas. The structure of the counterions also determines their distribution patterns. High-valent counterion units, driven by strong electrostatic forces, preferentially localize in the inner regions of the PE coronas near the hydrophobic cores, resulting in charge overcompensation and local charge inversion. However, long counterion chains, due to their extended structure, not only intensify the distribution of charge across the inner region but also effectively extend it to the outer edges of the coronas. Despite reduced total correlations from electrostatic screening within the counterion chains, the extended structure accommodates more PE monomers, potentially increasing the coordination number around the ion chains beyond that of multivalent units. The enhancement of the counterion chain backbone's rigidity diminishes their conformational entropy, prompting the emergence of a greater number of PE clusters. Additionally, the PE chains are extended to facilitate more effective adsorption by the inflexible counterion chains. In nature, the valence of an individual ion is inherently restricted, yet the number of monovalent ions in a chain can reach

https://doi.org/10.1021/acsomega.5c00002
ACS Omega 2025, 10, 17694−17704

significantly elevated levels, and a discussion of the effect of their structure is of practical importance.

■ ASSOCIATED CONTENT

Supporting Information

The Supporting Information is available free of charge at https://pubs.acs.org/doi/10.1021/acsomega.5c00002.

Snapshots of self-assembled structures in the presence of monovalent counterions, the RDFs between hydrophobic-PE monomers, processes of micellar cross-linking, PE clusters, calculation of diffusion coefficients, dynamic interconversion structures, pressure contributed from bond and kinetic energies, variation of condensation ratios and energies with simulation time, snapshots of self-assembled structures with different rigidities, and condensation ratios with different rigidities of counterion chains. (PDF)

■ AUTHOR INFORMATION

Corresponding Author

Liyan Liu − *College of Science, Civil Aviation University of China, Tianjin 300300, China;* orcid.org/0000-0003-4692-3882; Email: llypaper@126.com

Authors

Fujia Wang − *College of Science, Civil Aviation University of China, Tianjin 300300, China*

Boyi Zhang − *School of Biomedical Engineering and Technology, Tianjin Medical University, Tianjin 300070, China*

Ting Zhang − *School of Biomedical Engineering and Technology, Tianjin Medical University, Tianjin 300070, China*

Ying Wang − *School of Biomedical Engineering and Technology, Tianjin Medical University, Tianjin 300070, China*

Bing Han − *College of Science, Civil Aviation University of China, Tianjin 300300, China*

Complete contact information is available at: https://pubs.acs.org/10.1021/acsomega.5c00002

Author Contributions

[§]L.L. and F.W. are cofirst authors of the article.

Notes

The authors declare no competing financial interest.

■ ACKNOWLEDGMENTS

The authors are grateful for the financial support provided by the Natural Science Foundation of Tianjin City (No. 22JCZDJC00010).

■ REFERENCES

(1) Fehér, B.; Zhu, K. Z.; Nyström, B.; Varga, I.; Pedersen, J. S. Effect of temperature and ionic strength on micellar aggregates of oppositely charged thermoresponsive block copolymer polye:lectrolytes. *Langmuir* **2019**, *35*, 13614−13623.

(2) Huo, H. Y.; Zhao, W. C.; Duan, X. Z.; Sun, Z. Y. Control of diblock copolyelectrolyte morphology through electric field application. *Macromolecules* **2023**, *56*, 1065−1076.

(3) Duan, X.; Shi, A. C.; An, L. Formation of ionomer microparticles via polyelectrolyte complexation. *Macromolecules* **2021**, *54*, 9053−9062.

(4) Kienle, D. F.; Schwartz, D. K. Complex salt dependence of polymer diffusion in polyelectrolyte multilayers. *J. Phys. Chem. Lett.* **2019**, *10*, 987−992.

(5) Gulati, A.; Jacobs, M.; Lopez, C. G.; Dobrynin, V. Salt effect on the viscosity of semidilute polyelectrolyte solutions: sodium polystyrenesulfonate. *Macromolecules* **2023**, *56*, 2183−2193.

(6) Ortiz, J. A.; Sepúlveda, F. A.; Panadero-Medianero, C.; Murgas, P.; Ahumada, M.; Palza, H.; Matsuhiro, B.; Zapata, P. A. Cytocompatible drug delivery hydrogels based on carboxymethylagarose/chitosan pH-responsive polyelectrolyte complexes. *Int. J. Biol. Macromol.* **2022**, *199*, 96−107.

(7) Copp, S. M.; Hamblin, R. L.; Swingle, K.; Rai, D.; Urban, V. S.; Ivanov, S. A.; Montaño, G. A. Complex pH-dependent interactions between weak polyelectrolyte block copolymer micelles and molecular fluorophores. *Langmuir* **2022**, *38*, 2038−2045.

(8) Gao, X. J.; He, Z. X.; Ni, W. F.; Jian, X. Q.; Hu, C. H.; Zhao, Y. Q.; Yan, Y.; Wei, X. Layer-by-Layer Assembly of Functional Nanoparticles for Hepatocellular Carcinoma Therapy. *Adv. Funct. Mater.* **2019**, *29*, No. 1904246.

(9) Gao, X. J.; Bao, K.; Zhang, Y. Q.; Liu, L. Y.; Li, Y.; Hu, C. H.; Zhao, Y. Q.; Lu, W.; Wei, X. The Synergistic Effects of Multidrug-Loaded Nanocarriers Improve Tumor Microenvironment Responsive Chemo-Sonodynamic Therapy of Hepatocellular Carcinoma. *Adv. Funct. Mater.* **2023**, *33*, No. 2215014.

(10) Pimenta, B. V.; Madrid, R. R. M.; Mathews, P. D.; Riske, K. A.; Loh, W.; Angelov, B.; Angelov, A.; Mertins, O. Interaction of polyelectrolyte-shell cubosomes with serum albumin for triggering drug release in gastrointestinal cancer. *J. Mater. Chem. B* **2023**, *11*, 2490−2503.

(11) Kim, M.; Yeo, S. J.; Highley, C. B.; Burdick, J. A.; Yoo, P. J.; Doh, J.; Lee, D. One-step generation of multifunctional polyelectrolyte microcapsules via nanoscale interfacial complexation in emulsion (NICE). *ACS Nano* **2015**, *9*, 8269−8278.

(12) Hadadpour, M.; Gwyther, J.; Manners, I.; Ragogna, P. J. Multifunctional block copolymer: where polymetallic and polyelectrolyte blocks meet. *Chem. Mater.* **2015**, *27*, 3430−3440.

(13) Lin, C.; Qiang, X.; Dong, H. L.; Huo, J.; Tan, Z.-J. Multivalent ion-mediated attraction between like-charged colloidal particles: nonmonotonic dependence on the particle charge. *ACS Omega* **2021**, *6*, 9876−9886.

(14) Angelescu, D. G.; Linse, P. Monte Carlo simulation of the mean force between two like-charged macroions with simple 1:3 salt added. *Langmuir* **2003**, *19*, 9661−9668.

(15) Karayianni, M.; Pispas, S. Block copolymer solution self-assembly: Recent advances, emerging trends, and applications. *J. Polym. Sci.* **2021**, *59*, 1874−1898.

(16) Kötz, J.; Kosmella, S.; Beitz, T. Self-assembled polyelectrolyte systems. *Prog. Polym. Sci.* **2001**, *26*, 1199−1232.

(17) Cornelissen, J. J. L. M.; Fischer, M.; Sommerdijk, N. A. J. M.; Nolte, R. J. M. Helical superstructures from charged poly (styrene)-poly (isocyanodipeptide) block copolymers. *Science* **1998**, *280*, 1427−1430.

(18) Dobrynin, A. V. Theory and simulations of charged polymers: From solution properties to polymeric nanomaterials. *Curr. Opin. Colloid Interface Sci.* **2008**, *13*, 376−388.

(19) Sing, C. E.; Zwanikken, J. W.; de la Cruz, M. O. Interfacial behavior in polyelectrolyte blends: Hybrid liquid-state integral equation and selfconsistent field theory study. *Phys. Rev. Lett.* **2013**, *111*, No. 168303.

(20) Bagchi, D.; Nguyen, T. D.; de la Cruz, M. O. Surface polarization effects in confined polyelectrolyte solutions. *Proc. Natl. Acad. Sci. U.S.A.* **2020**, *117*, 19677−19684.

(21) Sing, C. E.; Zwanikken, J. W.; de la Cruz, M. O. Electrostatic control of block copolymer morphology. *Nat. Mater.* **2014**, *13*, 694−698.

(22) Zhang, P. F.; Alsaifi, N. M.; Wu, J. Z.; Wang, Z.-G. Salting-out and salting-in of polyelectrolyte solutions: A liquid-state theory study. *Macromolecules* **2016**, *49*, 9720−9730.

(23) Wang, F. J.; Liu, X. Y.; Yang, W.; Chen, Y.; Liu, L. Y. Responses of assembled structures of block polyelectrolytes to electrostatic interaction strength. *J. Chem. Phys.* **2024**, *160*, No. 144903.
(24) Liu, L. Y.; Wang, F. J.; Liu, X. Y.; Guo, L. D.; Gao, X. J.; Tan, H. G. Self-assembly of amphiphilic polyelectrolytes in trivalent salt solution. *Phys. Chem. Chem. Phys.* **2023**, *25*, 10042−10053.
(25) Li, N. K.; Kuang, H. H.; Fuss, W. H.; Zauscher, S.; Kokkoli, E.; Yingling, Y. G. Salt Responsive Morphologies of ssDNA-Based Triblock Polyelectrolytes in Semi-Dilute Regime: Effect of Volume Fractions and Polyelectrolyte Length. *Macromol. Rapid Commun.* **2017**, *38*, No. 1700422.
(26) Lin, C. J.; Wei, H.; Li, H. F.; Duan, X. Z. Structures of cationic and anionic polyelectrolytes in aqueous solutions: the sign effect. *Soft Matter* **2022**, *18*, 1603−1616.
(27) Pochan, D. J.; Chen, Z.; Cui, H.; Hales, K.; Qi, K.; Wooley, K. Toroidal triblock copolymer assemblies. *Science* **2004**, *306*, 94−97.
(28) Liu, L.; Pincus, P. A.; Hyeon, C. Heterogeneous morphology and dynamics of polyelectrolyte brush condensates in trivalent counterion solution. *Macromolecules* **2017**, *50*, 1579−1588.
(29) Tan, H.-G.; Xia, G.; Liu, L.-X.; Miao, B. Morphologies of a polyelectrolyte brush grafted onto a cubic colloid in the presence of trivalent ions. *Phys. Chem. Chem. Phys.* **2019**, *21*, 20031−20044.
(30) Gordievskaya, Y. D.; Kramarenko, E. Y. Effect of counterion size on the structure of a flexible polyelectrolyte chain in low-polar solvents. *Polym. Sci., Ser. C* **2018**, *60*, 37−48.
(31) Bodrova, A. S.; Potemkin, I. I. Influence of the counterion size on swelling and collapse of polyelectrolyte gel. *Polym. Sci., Ser. A* **2007**, *49*, 737−744.
(32) Butler, J. C.; Angelini, T.; Tang, J. X.; Wong, G. C. L. Ion multivalence and like-charge polyelectrolyte attraction. *Phys. Rev. Lett.* **2003**, *91*, No. 028301.
(33) Wyatt, N. B.; Liberatore, M. W. The effect of counterion size and valency on the increase in viscosity in polyelectrolyte solutions. *Soft Matter* **2010**, *6*, 3346−3352.
(34) Tan, H.-G.; Guo, L.-D.; Qian, H.-Y.; Liu, L.-X.; Hao, Q.-H.; Miao, B. Size Effect of Multivalent Counterions on Polyelectrolyte Brushes in Different Polar Solvents. *Macromolecules* **2023**, *56*, 9312−9323.
(35) Gavrilov, A. A. Effect of the counterion size on microphase separation in charged-neutral diblock copolymers. *J. Chem. Phys.* **2023**, *158*, No. 054901.
(36) Cui, H.; Chen, Z.; Wooley, K. L.; Pochan, D. J. Controlling micellar structure of amphiphilic charged triblock copolymers in dilute solution via coassembly with organic counterions of different spacer lengths. *Macromolecules* **2006**, *39*, 6599−6607.
(37) Akisada, H.; Ishihara, M.; Nishi, M.; Higake, M.; Ishimaru, S.; Nisida, J. Chain length effect of the counterion on the partial molal volume of alkanesulfonates. *Colloid Polym. Sci.* **2003**, *281*, 993−997.
(38) Cui, H.; Chen, Z.; Wooley, K. L.; Pochan, D. J. Origins of toroidal micelle formation through charged triblock copolymer self-assembly. *Soft Matter* **2009**, *5*, 1269−1278.
(39) Kremer, K.; Grest, G. S. Dynamics of entangled linear polymer melts: A molecular-dynamics simulation. *J. Chem. Phys.* **1990**, *92*, 5057−5086.
(40) Murat, M.; Grest, G. S. Molecular dynamics study of dendrimer molecules in solvents of varying quality. *Macromolecules* **1996**, *29*, 1278−1285.
(41) Sandberg, D. J.; Carrillo, J. M. Y.; Dobrynin, A. V. Molecular dynamics simulations of polyelectrolyte brushes: From single chains to bundles of chains. *Langmuir* **2007**, *23*, 12716−12728.
(42) Cao, Q. Q.; Zuo, C. C.; Li, L. J.; Zhang, N. Conformational Behavior of Bottle-Brush Polyelectrolytes with Charged and Neutral Side Chains. *Macromol. Theory Simul.* **2010**, *19*, 298−308.
(43) Frenkel, D.; Smit, B.; Ratner, M. A. Understanding Molecular Simulation: From Algorithms to Applications. *Phys. Today* **1997**, *50*, 66.
(44) Plimpton, S. Fast parallel algorithms for short-range molecular dynamics. *J. Comput. Phys.* **1995**, *117*, 1−19.
(45) Grest, G. S.; Kremer, K. Molecular dynamics simulation for polymers in the presence of a heat bath. *Phys. Rev. A* **1986**, *33*, 3628.
(46) Paterlini, M. G.; Ferguson, D. M. Constant temperature simulations using the Langevin equation with velocity Verlet integration. *Chem. Phys.* **1998**, *236*, 243−252.
(47) Thompson, A. P.; Aktulga, H. M.; Berger, R.; Bolintineanu, D. S.; Brown, W. M.; Crozier, P. S.; in 't Veld, P. J.; Kohlmeyer, A.; Moore, S. G.; Nguyen, T. D.; Shan, R.; Stevens, M. J.; Tranchilda, J.; Trott, C.; Plimpton, S. J. LAMMPS-a flexible simulation tool for particle-based materials modeling at the atomic, meso, and continuum scales. *Comput. Phys. Commun.* **2022**, *271*, No. 108171.
(48) Stillinger, F. H., Jr. Rigorous basis of the frenkel-band theory of association equilibrium. *J. Chem. Phys.* **1963**, *38*, 1486−1494.
(49) Liu, L.-Y.; Xia, G.; Feng, Z.-J.; Hao, Q.-H.; Tan, H.-G. Self-assembly of polyelectrolyte diblock copolymers at monovalent and multivalent counterions. *Soft Matter* **2019**, *15*, 3689−3699.
(50) Cahoon, J. R. The first coordination number for liquid metals. *Can. J. Phys.* **2004**, *82*, 291−301.
(51) Headen, T. F.; Boek, E. S.; Skipper, N. T. Evidence for asphaltene nanoaggregation in toluene and heptane from molecular dynamics simulations. *Energy Fuels* **2009**, *23*, 1220−1229.
(52) Einstein, A. Über die von der molekularkinetischen Theorie der Wärme geforderte Bewegung von in ruhenden Flüssigkeiten suspendierten Teilchen. *Ann. Phys.* **1905**, *322*, 549−560.
(53) Yu, J.; Jackson, N. E.; Xu, X.; Brettmann, B. K.; Ruths, M.; De Pablo, J. J.; Tirrell, M. Multivalent ions induce lateral structural inhomogeneities in polyelectrolyte brushes. *Sci. Adv.* **2017**, *3*, No. eaao1497.
(54) Chen, X.; Chen, E. Q.; Yang, S. Multivalent counterions induced attraction between DNA polyelectrolytes. *RSC Adv.* **2020**, *10*, 1890−1900.
(55) Thompson, A. P.; Plimpton, S. J.; Mattson, W. General formulation of pressure and stress tensor for arbitrary many-body interaction potentials under periodic boundary conditions. *J. Chem. Phys.* **2009**, *131*, No. 154107.
(56) Qin, L.; Xie, Q. J.; Bao, J. W.; Sant, G.; Chen, T. F.; Zhang, P.; Niu, D. T.; Gao, X. J.; Bauchy, M. Investigation of Carbonation Kinetics in Carbonated Cementitious Materials by Reactive Molecular Dynamics Simulations. *ACS Sustainable Chem. Eng.* **2024**, *12*, 10075−10088.
(57) Ghelichi, M.; Qazvini, N. T. Self-organization of hydrophobic-capped triblock copolymers with a polyelectrolyte midblock: A coarse-grained molecular dynamics simulation study. *Soft Matter* **2016**, *12*, 4611−4620.

https://doi.org/10.1021/acsomega.5c00002
ACS Omega 2025, 10, 17694−17704